Plasmonics (2017) 12:783–794
DOI 10.1007/s11468-016-0325-z

Gold-Graphene Core-Shell Nanostructure Surface Plasmon Sensors

Raed Alharbi[1,2] · **Mehrdad Irannejad**[1,2] · **Mustafa Yavuz**[1,2]

Received: 27 April 2016 / Accepted: 29 June 2016 / Published online: 9 July 2016
© Springer Science+Business Media New York 2016

Abstract Localized surface plasmon resonance sensors in nanostructures have wide applications from medical diagnostics to environmental monitoring. The quality and performance of a sensor is normally assessed by its sensitivity and figure of merit (FOM). Generally, localized surface plasmon sensors suffer low FOM due to strong radiative damping of localized surface plasmon and hence broad resonance peaks compared to that one in propagating surface plasmon resonance sensors. In this work, a 2D array of gold-graphene spherical core-shell nanostructure on a quartz substrate was introduced as a liquid sensor with FOM and sensitivity as large as 102.6 and 350 nm/RIU, respectively, in a gold-graphene hybrid nanostructure. The results showed a significant improvement in the FOM compared to previous works and common surface plasmon resonance refractive index surface plasmon sensors such as nanohole arrays.

Keywords Surface plasmon · Quantum dots · Sensitivity · Figure of merit · Graphene · Biosensor

Introduction

Surface plasmon resonance (SPR) is a well-known phenomenon used in chemical/bio sensing applications such as medical diagnostics, food safety, and environmental monitoring [1, 2]. The SPR sensors work based on the surface plasmon evanescent waves coupling with incident electromagnetic field, called surface plasmon polariton (SPP). The SPP is sensitive to the permittivity variation of the ambient environment that resulted in a measurable wavelength shift in the SPP position and the resonant intensity [3, 4]. The quality and quantity performance of a SPR sensor can be carried out by considering the bulk sensitivity, figure of merit (FOM), and the contrast of the nanostructure. The bulk sensitivity is defined as the resonance wavelength shift divided by the refractive index change ($S = \Delta\lambda/\Delta n$) of the ambient environment, and the FOM can be calculated from [5];

$$\mathrm{FOM} = S/\mathrm{FWHM} \tag{1}$$

where S and FWHM are the sensitivity and full width at half maximum of the resonance peaks, respectively. The contrast which is defined as the difference between reflection values at the dip and adjacent peaks [4] can be used in analysis of reflection spectrum of nanostructures.

Simplicity, low fabrication cost, and capability of local refractive index measurement make localized surface plasmon resonance (LSPR) sensor superior than propagated surface plasmon resonance (PSPR) sensors [6, 7]. However, due to strong radiative damping of LSP modes, the width of the resonance peaks in the LSPR sensors is larger than that in the PSPR sensors which results in a reduction in the FOM of the sensor [5, 8, 9]. Therefore, LSPR-based sensors suffer from low value of FOM (normally less than 10) [7, 10] compared to that in a PSPR sensor which was reported as 108 [11]. With coupling the LSPR and PSPR of nanostructure, higher sensitivity and FOM can be achieved in hybrid surface plasmon resonance sensors [6, 7].

In order to enhance the sensor performance, a resonance peak with large sensitivity and small FWHM is required to

✉ Mehrdad Irannejad
mehrdad.irannejad@uwaterloo.ca

[1] Waterloo Institute for Nanotechnology, University of Waterloo, Waterloo, ON, Canada

[2] Mechanical and Mechatronics Engineering, University of Waterloo, Waterloo, ON, Canada

end up with high FOM. There are many different ways to reduce the FWHM and hence increasing the FOM of a LSPR sensor. Using Fano resonance mode is an effective way to enhance the FOM due to formation of a resonance mode with narrow FWHM as a result of coupling between broad superradiant and narrow subradiant modes [11]. Split ring resonator-bar structures [12], lifted cross-bar structures [13], closely packed nanodisk clusters [14], and silver nanocube supported on dielectric substrates [5] are some examples of common nanostructure sensors that use the Fano resonance phenomenon with FOM in the range of 5 to 20.

Fabrication of 1D or 2D periodic nanostructure arrays could be considered as an alternative way to enhance the FOM of a LSPR sensor [15–19] where the lattice plasmon resonances (i.e., resonances resulting from an array of nanoparticles) with FWHM as low as 10 nm can be achieved via coupling between the diffraction patterns of different periodic arrays of nanoparticles [16–18].

Recently, Wang and co-workers [20] study the lattice plasmon of single and multiple periodic arrangements of Au nanoparticles. It was shown that the periodic patches of Au nanoparticles resulted in narrower resonance peaks than a single patch of Au nanoparticles. The observation of strong and narrower plasmon resonance peaks in the periodic patches of Au nanoparticles was due to the coupling between the lattice plasmon resonances of the Au nanoparticles and Bragg modes that are defined by the patch periodicity.

In addition to the aforementioned techniques to enhance the FOM, nanoparticle geometrical parameters, shape, and material properties play an essential role in the sensor performance. Gold (Au) and silver (Ag) are most two common materials in surface plasmon sensors which have surface plasmon resonance wavelength in visible range of the electromagnetic spectrum and offer narrow resonance peaks in the desired region [21, 22]. Graphene and its derivatives are one of the promising candidates as surface plasmon excitation materials in a surface plasmon sensor technology due to their unique electronic and optical properties [23].

The graphene layer can be combined with conventional plasmonic nanostructures to improve the interaction between the graphene and electromagnetic wave. There are few reports that show the encapsulation of spherical nanoparticles by ablating the graphene in liquid using high-power pulsed lasers. The laser ablation in liquid is capable of producing encapsulated nanoparticles with anisotropic graphene layer [24]. Plasmonic material encapsulation with graphene layer could also be carried out by placing the graphene in different kinds of optical microcavities [25] and fabrication of patterned graphene islands periodically [26].

Graphene has a strong plasmonic response at mid-far infrared region which limits its application in detection and sensing in the visible-near-infrared (NIR) region of the electromagnetic spectrum [27–29]. Although graphene has a constant wavelength-independent absorption at the visible-NIR region, absorption enhancement is required in order to have a potential application in optical devices [30]. For example, the graphene absorption can be enhanced by placing a graphene layer in different micro- or nanocavities such as integrating the graphene with metal (e.g., Ag) grating and Si photonic crystal cavity where 70 and 85 % enhancement can be achieved in its absorption, respectively [30, 31]. Increasing the graphene absorption results in a narrower absorption peak and hence larger FOM of the sensor. Maurer et al. [32] employed graphene as a spacer between the Au film and Au nanoparticles to obtain larger FOM relative to that one without graphene spacer.

Furthermore, the size and geometry of the nanoparticle are another two main parameters that affect the sensitivity and the FOM of a LSPR sensor [1, 3, 4]. There are many reported LSPR sensors with different nanoparticle shapes such as nanosphere [33, 34], nanocube [5], nanoprism [34], nanopyramid [35], nanoring [36], and nanobelt [37] all of which with FOM as low as 20.

Recently, core-shell structure brought into the attention where the surface plasmon resonance modes resulted from this structure can be coupled together and resulted in enhanced hybrid plasmon modes. For example, Yang et al. [38] and Christensen et al. [39] explained the plasmon interaction of dielectric and conductive sphere (core) coated by graphene layer. In this structure, the coupling between the surface plasmon modes of the core and shell structures can be explained by hybridization theory [40] where the plasmon resonances resulted from the interaction of the sphere and cavity plasmons give bonding (symmetric) and antibonding (antisymmetric) modes. Bonding mode offers high dipole moment and hence can be easily coupled with incident light that lead to stronger plasmon absorption than antibonding mode which can be used in sensing applications.

Encapsulating Au nanoparticles by graphene oxide (GO) layer on a silica substrate was reported by Sreejith and coworkers [41]. The Au nanoparticles were encapsulated by GO using electrostatic interaction between the positively charged quartz surface and negatively charged GO resulting in plasmonic nanohybrid GO/Au nanoparticle on the quartz substrate. The plasmonic properties of this structure were studied at visible range of electromagnetic spectrum and an enhancement in the absorption reported using the finite difference time domain (FDTD) analysis which was contributed to the contribution of GO sheets in the nanostructure. In addition, Han et al. [42] reported a peptide/graphene hybrid core/shell nanowire structure. Peptide/graphene core/shell nanowires were prepared by diluting an organic peptide solution with aqueous graphene dispersion under mild mechanical shaking. The peptide/graphene exhibited high electro conductivity properties due to continuous graphene shell.

Choosing a suitable wavelength range is one of the important parameters in designing the nanosensors that are used in in vivo measurements [43]. To detect a biomarker of cancer cell such as breast cancer, blood serum is used to detect the concentration of that biomarker. Due to the transmissivity of the blood and tissue and strong absorption of water, we study a nanobiosensor in the NIR region [44]. Moreover, by using NIR wavelengths, the autofluorescence effect that was caused by some biomolecule (e.g., hemoglobin) and light scattering by tissue at visible range could be prevented [43].

In this work, the effects of using different parameters such as periodicity, diameter, and thickness of the Au-graphene hybrid nanostructure on the sensitivity and FOM of a LSPR sensor are studied. A series of periodic arrays of the Au-graphene spherical core-shell nanostructure on a quartz substrate were studied numerically as local refractive index sensor for liquids. The refractive index variation is considered in the range of 1.333 to 1.373, and the sensitivity and FOM of the designed structure are calculated using the FDTD method.

The proposed sensor could be fabricated by using following steps: (i) The Au nanoparticle arrays with particle diameter (d) in the range of 40 to 60 nm were fabricated on a quartz substrate using electron beam lithography technique as discussed in details elsewhere [45]. (ii) The fabricated nanostructure was covered with a thin layer of multilayer (less than 10 layers) graphene nanopowder followed by thermal annealing under controlled environment as discussed in details by [46]. (iii) In the last step, lithography and the reactive ion etching were employed to remove graphene nanopowders from the area between the hybrid nanostructures [47, 48].

Numerical Model and Layout

There are many different methods to study the electromagnetic field behavior numerically around nanofeatures such as multiple-multiple method [49], Green's dynamic method [50, 51], and FDTD [37, 52–54] which is a reliable method in solving Maxwell's equations in complex geometries and dispersive media such as gold and silver.

In this work, the 3D full wavevector FDTD method was employed to solve the Maxwell equation and calculate the extinction spectra of gold-graphene (Au-G) hybrid nanostructure arrays placed on top of a silica substrate as schematically shown in Fig. 1. The permittivity of glass substrate and superstrate (i.e., target materials for sensing application), $\varepsilon(\omega)$, was assumed as 2.10 (n = 1.45) and n_i, where n_i is the refractive index of the target liquids.

The refractive index values of gold and graphene were calculated using the Lorentz-Drude model and fitted with the empirical values of real and imaginary part of gold refractive index given by [55] and graphene which was obtained from the Falkovsky model [56], over the wavelength region of 1 to 1.5 μm as shown in Fig. 2.

The numerical analysis was carried out using the FDTD commercial software package (Lumerical FDTD Solutions). The Au-G hybrid nanostructure, plane wave source, and transmission and reflection monitors were co-planar with the boundary conditions that made them infinite in the x- and y-directions. Herein, an unpolarized plane electromagnetic wave in the wavelength range of 1 to 1.5 μm with electric field amplitude of 1 V/m which propagates in the z-axis (as labeled by arrows in Fig. 1) was used as incident light source.

The periodic boundary conditions in the x- and y-directions can be replaced by the asymmetric and symmetric boundary conditions in the x- and y-directions, respectively, in order to reduce the calculation time [57]. The perfect matching layer (PML) was chosen in the z-direction to study the transmission and reflection properties of the electromagnetic field at normal incidence. The calculation grid resolution (i.e., mesh cell size) was as small as 5 nm (point-to-point distance) in the x- and y-directions and 1 nm in the z-direction in the simulation cell. A combination of grading mesh and conformal meshing method which is offered by the Lumerical FDTD package was used to calculate the electromagnetic field at the rounded region of the Au-G hybrid nanostructures [57]. The calculation time was set as 3000 fs, and the extinction spectra were calculated using an

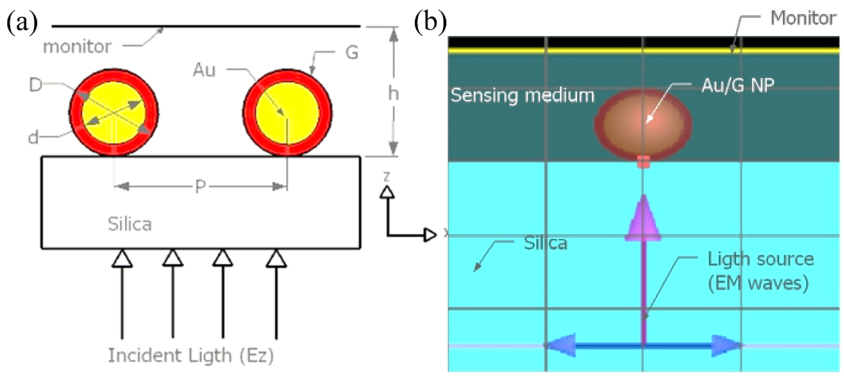

Fig. 1 2D **a** schematic diagram and **b** numerical layout of the designed sensor used in this study. D is the Au-G hybrid nanostructure diameter, d is the Au nanoparticle diameter, t is the graphene thickness ($t = D/2 - d/2$), and P is the structural periodicity

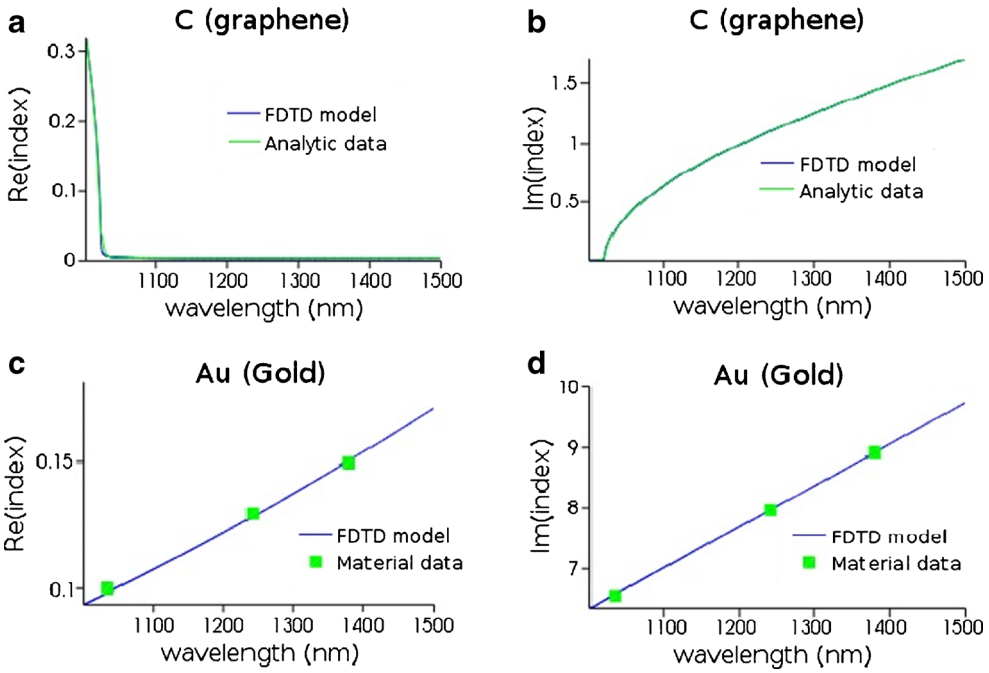

Fig. 2 Real part and imaginary part of **a**–**b** graphene refractive index and **c**–**d** gold refractive index based on the Lorentz-Drude mode as a function of wavelength in the range of 1 to 1.5 μm. The experimental and analytical refractive indices were taken from [55] and [56] for gold and graphene, respectively

x-*y* monitor at 150 nm away from the Au-G /superstrate (liquid) interface. The plane wave source was placed 150 nm below the structure as shown in Fig. 1.

There are many parameters such as scattering rate and chemical potential which affect the electrical permittivity and hence refractive index of the graphene at different wavelengths in the NIR region as reported by Falkovsky [56]. In this study, the electrical permittivity of graphene at room temperature and different wavelengths was taken from the Falkovsky model. The background refractive index was chosen as 1 (air), and water (n = 1.333) was used as reference liquid in the sensitivity and FOM measurements.

Herein, a series of Au-G hybrid nanostructures were studied with different structural periodicities (P), Au diameter (d), and graphene thickness ($t = D/2 - d/2$), while the total size of the hybrid nanostructure (D) was fixed. The optimum parameters were obtained for a structure with the highest extinction ($1 - T$) intensity and narrower resonance peak. The sensitivity and FOM of the Au-G hybrid nanostructure with optimum parameters were calculated by changing the target liquid refractive indices in the range of 1.333 to 1.373.

Results and Discussion

The Effects of Graphene Contribution on the Au Nanostructure Extinction Spectrum

The effects of graphene contribution on the surface plasmon resonance properties of the Au nanostructure periodic array in the NIR region were investigated by calculating the extinction ($1 - T$) spectrum of the Au-G hybrid nanostructures and compare it with that in the Au nanoparticle periodic arrays as shown in Fig. 3. The diameter of the Au nanoparticles was fixed at 40 nm, while in the second structure (i.e., Au-G hybrid nanostructure), the gold diameter and the graphene shell thickness (t; $t = D/2 - d/2$) were chosen as 34 and 3 nm, respectively, to fix the whole nanoparticle diameter at 40 nm as schematically shown in Fig. 1a. The structural periodicity for both nanostructures was fixed at 300 nm.

With comparison of Fig. 3a and Fig. 3b, it is evident that by introducing a 3-nm-thick graphene shell into the Au nanoparticle, the resonance mode at wavelengths of 1265 and 1442 nm were shifted to 1271 and 1409 nm, respectively. Additionally, a strong bonding hybrid resonance mode at a wavelength of 1363 nm was also recorded.

The presence of this resonance peaks could be attributed to the excitation of graphene surface plasmon in the nanostructure as a result of coupling between the incident light and grating mode in the Au-G hybrid nanostructure [30]. The resonance peaks at wavelengths of 1265 and 1442 nm were attributed to the LSPR resonance of the Au nanosphere.

As can be seen from Fig. 3a, b, the extinction spectrum of the Au-G hybrid nanostructures shows a more intense peak with 23 % extinction enhancement at a wavelength of 1363 nm which was absent in the Au nanosphere periodic array. The enhancement in the extinction at a wavelength of 1363 nm could be attributed to the surface plasmon energy transfer from the gold nanoparticle to the graphene shell and coupling between localized surface plasmons of each Au-G hybrid nanostructure in the periodic array as reported elsewhere [30].

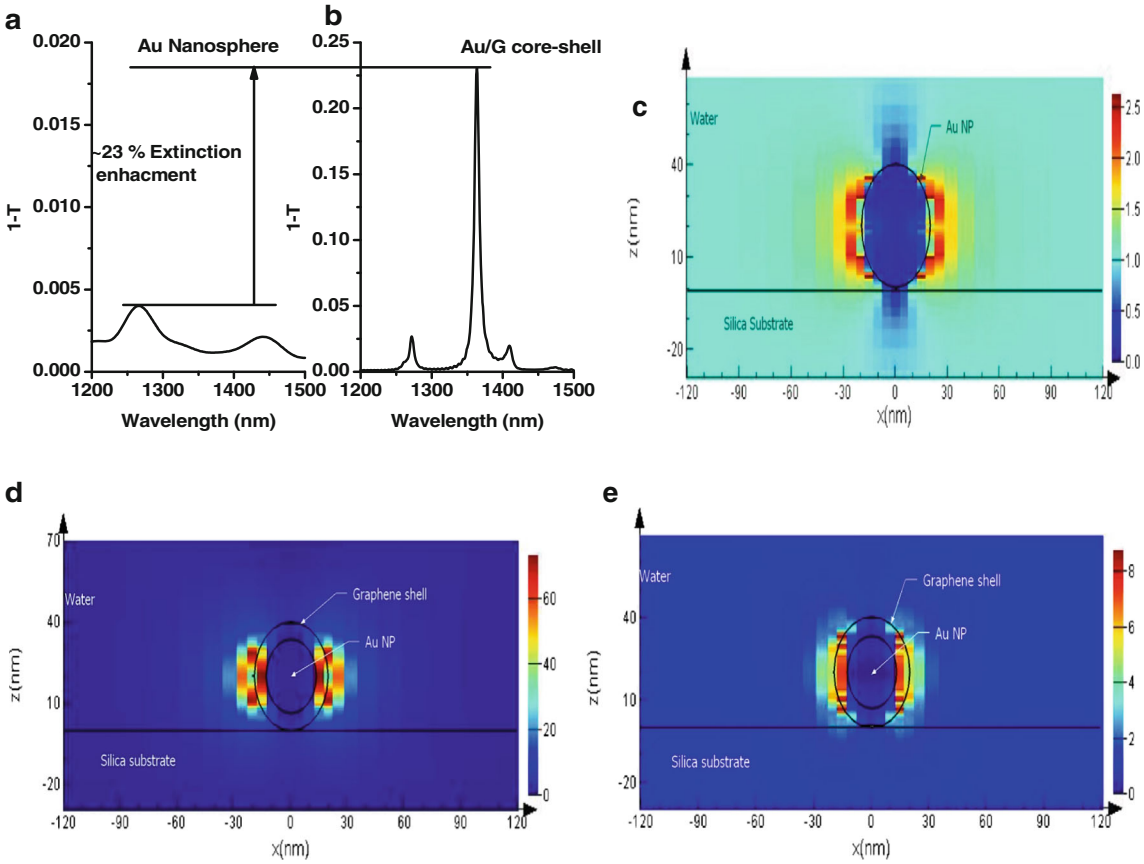

Fig. 3 Extinction spectrum of the **a** Au nanoparticle with a diameter of 40 nm and the **b** Au-G hybrid nanostructure with Au diameter of 37 nm and graphene shell thickness of 3 nm. In both structures, the structural periodicity and incident electric field amplitude was fixed at 300 nm and 1 V/m, respectively. **c**, **d** Electric field profile of Au nanoparticles at $\lambda = 1265$ nm (bonding) and Au-G hybrid nanostructure at $\lambda = 1272$ nm (antibonding), respectively. **e** The electric field profile of the Au-G hybrid nanostructure array structure at $\lambda = 1363$ nm (bonding)

In addition, the Au-G hybrid plasmonic resonances were observed as strong and weak resonance peaks which can be attributed to the bonding (B) and antibonding (AB) plasmon modes [40] The B and AB modes resulted from the interaction (hybridization) between the sphere and the plasmon cavity (i.e., graphene shell). However, the proposed structure (Au-G core-shell) includes hybridizations between the graphene shell and Au sphere that resulted from two steps of hybridization as reported elsewhere [58–60].

The electric profile at the resonance peaks of both Au nanoparticles and Au-G hybrid nanostructures is compared in Fig. 3c–e. As can be seen from Fig. 3c, d, the electric field amplitude was increased from 2.5 to 8.8 V/m at a resonance wavelength of 1265 nm by encapsulating the Au nanoparticle with 3-nm graphene. It is expected that introducing the graphene shell into the Au nanoparticle results in a slight red shift in the recorded resonance wavelength position of the hybrid nanostructure as it is shown in Fig. 3a, d.

The localization of the electric field was observed in the space between the graphene shell and Au nanoparticle instead of outside the graphene shell which can be attributed to the absorption characteristics of graphene where it has a constant absorption along the visible-IR range [30]. However, at the bonding mode at a wavelength of 1363 nm, the electric field enhancement increased to 73 V/m as it is clear from Fig. 3e. This enhancement in localized electric field results in improvement of local sensitivity of the refractive index changes and accordingly enhances the performance of the LSPR-based sensor.

The Effects of Varying the Structural Periodicity

To study the effects of varying the periodicity on the surface plasmon resonance properties of the proposed structure, a series of encapsulated Au sphere of a diameter of 34 nm with 3 nm thick graphene were studied numerically. The structural periodicity along the *x*-axis and *y*-axis were changed in the range of 300 to 500 nm with an increment step of 50 nm.

Figure 4a shows effects of varying the periodicity on the extinction spectrum of the Au-G hybrid nanostructure. As can be seen from this figure, there is no any shift in the resonance peak position which indicates that these resonances are localized surface plasmon resonance. The resonance wavelengths are independent of large separation compared with particle

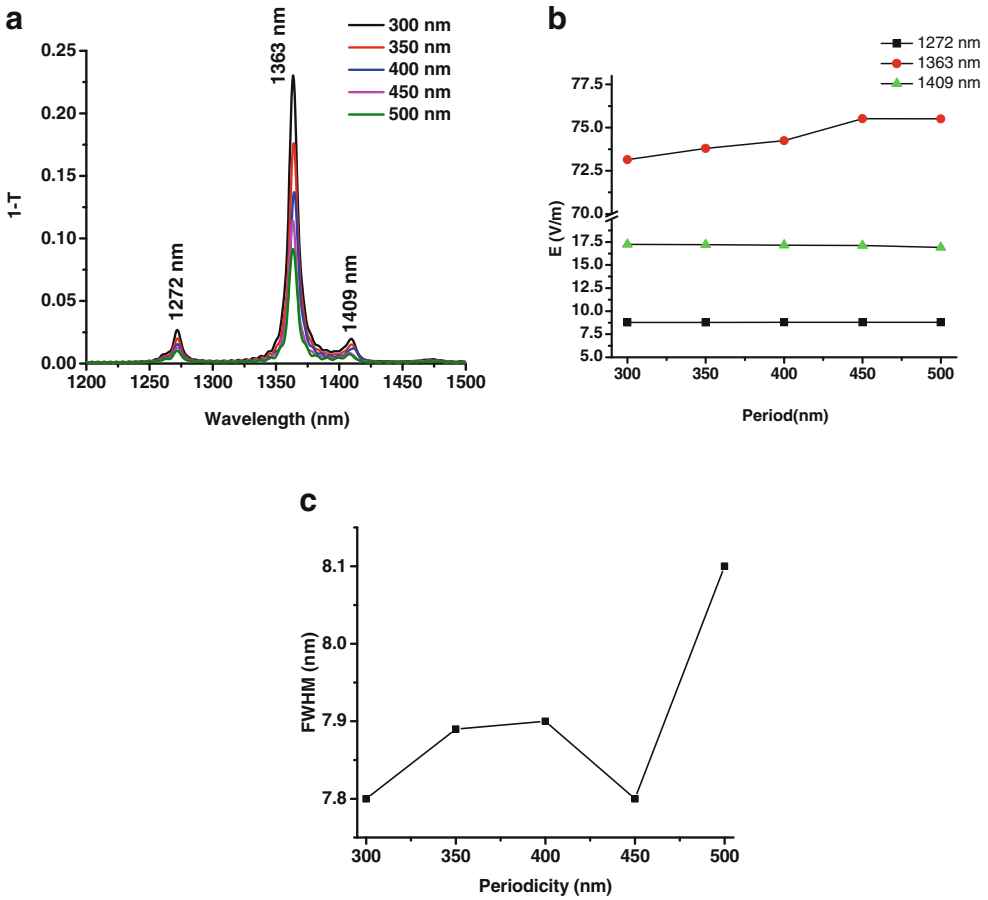

Fig. 4 **a** Extinction spectrum of the Au-G nanostructure array at different periodicities. **b** Electric field value as a function of structural periodicity at resonances at wavelengths of 1272, 1363, and 1409 nm. **c** The FWHM of the resonance wavelength of 1363 nm as function of structural periodicity. The incident electric field amplitude was fixed at 1 V/m. The Au nanoparticle diameter and graphene shell thickness were fixed at 34 and 3 nm, respectively

size as reported by Mayer and Hafner [6]. As it is clear from Fig. 4a, the intensity of the resonance peaks was gradually increased while the calculated FWHM of the resonance peak at a wavelength of 1363 nm was decreased from 8.1 to 7.8 nm as a result of reducing the structural periodicity from 500 to 300 nm as presented in Fig. 4c.

The increases in the resonance intensity at a resonance wavelength of 1363 nm can be attributed to the suppression of the scattered surface plasmon modes from the Au-G hybrid nanostructure at smaller structural periodicity and hence enhancement of the electric field amplitude localization at resonance position.

It was also observed that the extinction of the resonance mode at a wavelength of 1363 nm of the Au-G hybrid nanostructure was increased by 25 % as the periodicity decreases from 500 to 300 nm as it is clear from Fig. 4a. This can be attributed to the suppression of the scattered surface plasmon modes from the Au-G hybrid nanostructure at smaller structural periodicity and hence enhancement of the electric field amplitude localization at resonance position.

The maximum electric filed amplitude of the Au-G hybrid nanostructure at different resonance wavelengths of 1272, 1363, and 1409 nm as a function of structural periodicity is shown in Fig. 4b. As can be seen from this figure, there are no significant changes in the recorded electric field amplitude of each resonance wavelength at different periodicities.

Therefore, the structural periodicity of 300 nm was chosen as the optimum structural periodicity for an Au-G hybrid nanostructure due to its narrower band width and higher intensity compared to that with other structural periodicities. Further investigations were carried out to study the effects of varying the Au diameter and graphene thickness on the surface plasmon resonance properties of a refractive index sensor which are discussed in the following sections.

The Effects of Varying the Au Nanoparticle Size and Graphene Shell Thickness

The effects of varying both the Au nanoparticle diameter and graphene thickness on the surface plasmon properties of the hybrid nanostructure at a fixed structural periodicity of 300 nm and hybrid nanoparticle (i.e., Au diameter and graphene shell thickness) sizes of 40, 50, and 60 nm were studied. A series of different Au-G hybrid nanostructures with different Au diameters and graphene thicknesses in the range of 3 to 7 nm were studied, and their extinction spectra are shown in Fig. 5a–c.

The resonance wavelength, extinction, and FWHM of the bonding mode (i.e., resonance with maximum intensity) of the Au-G hybrid nanostructure with different Au diameters, with different graphene thicknesses, and using

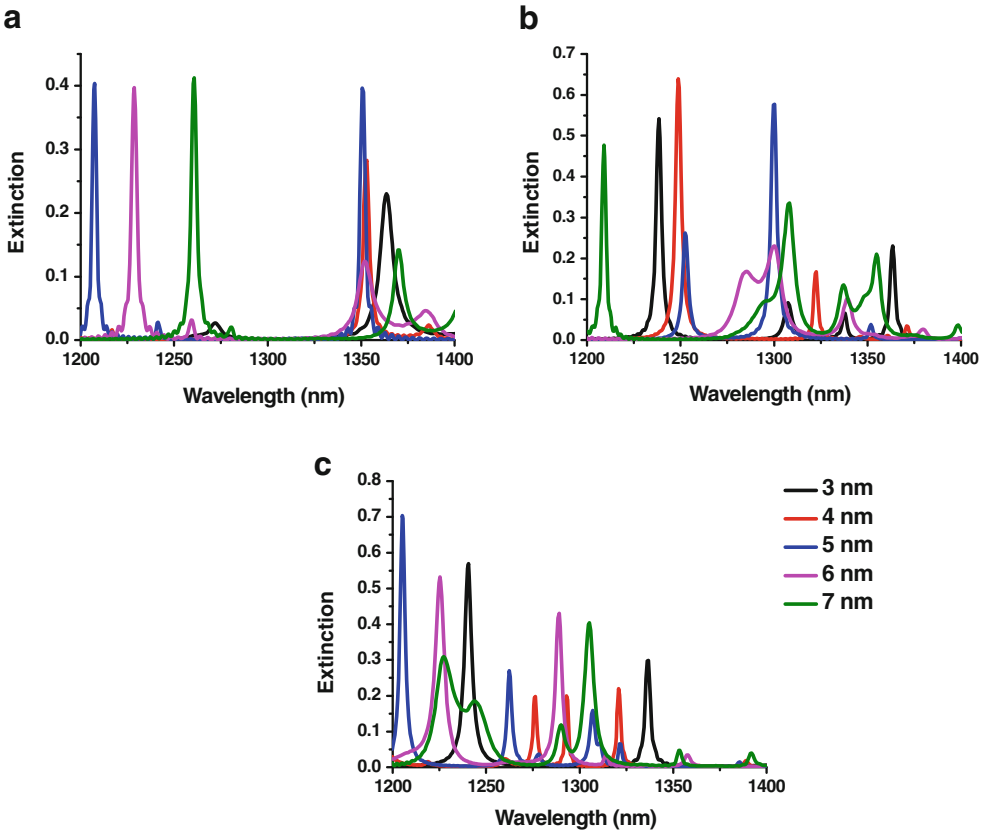

Fig. 5 Extinction spectra of the Au-G hybrid nanostructure with an Au-G hybrid nanostructure diameter of **a** 40 nm, **b** 50 nm, and **c** 60 nm and different graphene thicknesses in the range of 3 to 7 nm. The structural periodicity and incident electric filed amplitude were fixed at 300 nm and 1 V/m, respectively

water (n = 1.333) as superstrate medium are summarized in Table 1 and compared in Fig. 6a–c. As it is evident from this table and Fig. 6a–c, both Au diameter and graphene thickness significantly affected the resonance position and its intensity. As it is expected, the bonding and antibonding resonance wavelengths was blue shifted by increasing the graphene thickness from 3 to 7 nm. This blue shift in the resonance wavelength can be attributed to the weaker interaction between gold nanoparticle and graphene shell and hence smaller energy splitting of the bonding and antibonding plasmon modes in the hybrid nanostructure with thicker graphene shell [61].

As can be seen from Fig. 6a, the resonance wavelengths of encapsulated hybrid nanostructures with different graphene shell

Table 1 Resonance wavelength, extinction intensity, and FWHM of the bonding mode in the Au-G hybrid nanostructure with different Au diameter and graphene thicknesses

Total hybrid size (nm)	Graphene thickness (nm)	Resonance position (nm)	Extinction intensity	FWHM (nm)
40	3	1363	0.23	8.47
	4	1184	0.39	2.3
	5	1351	0.40	3.55
	6	1228	0.39	3.5
	7	1261	0.41	3.73
50	3	1239	0.54	3.13
	4	1248	0.64	2.2
	5	1300	0.58	3.63
	6	1180	0.38	3.13
	7	1209	0.48	2.61
60	3	1240	0.57	4.24
	4	1129	0.7	2.89
	5	1205	0.70	2.89
	6	1225	0.53	6
	7	1188	0.55	2.50

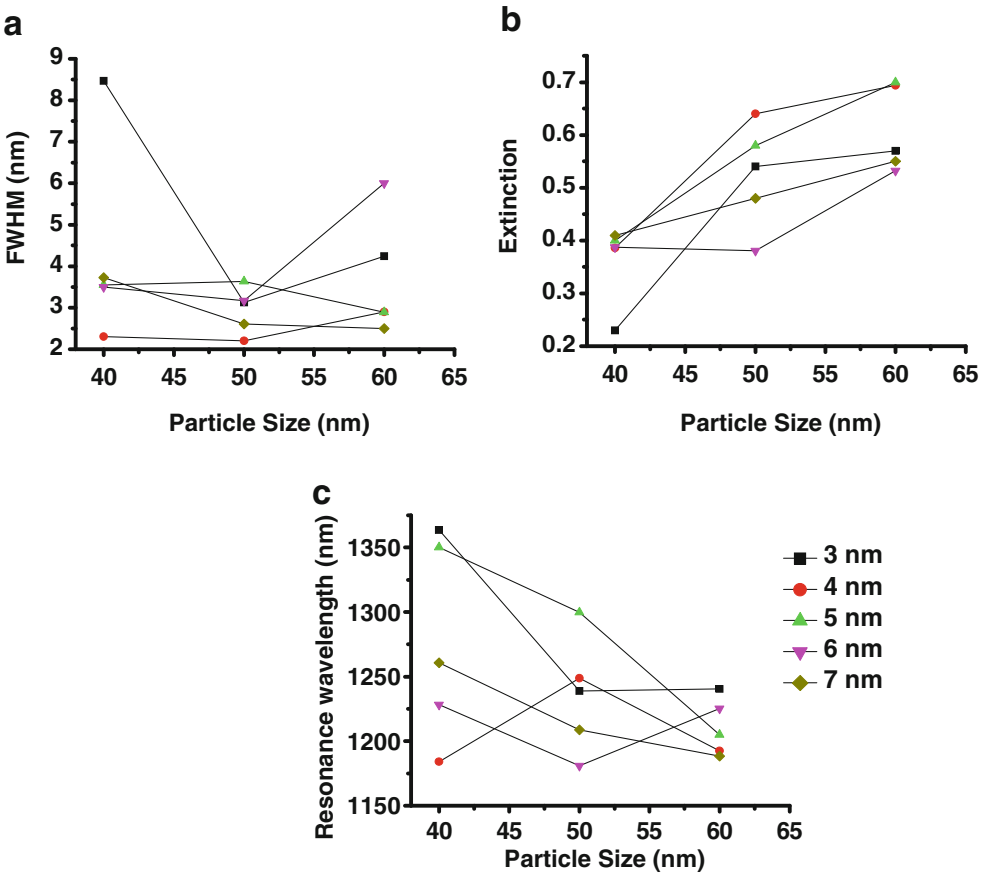

Fig. 6 **a** FWHM, **b** extinction intensity, and **c** the resonance wavelength of the bonding resonance mode of the Au-G hybrid nanostructure as a function of hybrid nanostructure diameter at different graphene thicknesses

thicknesses were shifted toward smaller wavelength by increasing the Au diameter while the extinction intensity was increased.

Increasing the electron density in the hybrid nanostructure could be another reason of this blue shift in the resonance wavelengths. Increasing the Au nanoparticle diameters results in larger electron density in the periodic array. The electron density and resonance wavelength can be related by [62]:

$$\lambda_b = \frac{c\sqrt{m_e \varepsilon_0}}{\sqrt{n_e e^2}} \tag{2}$$

where n_e is the electron density, e is the electric charge, m_e is the effective mass of the electron, ε_0 is the permittivity of free space, and c is the speed of light. As it is evident from this equation by increasing the electron density, the resonance wavelength decreases which results in a blue shift in the resonance wavelength of the hybrid nanostructure.

The resonance peak intensity and its FWHM strongly depend on the nanoparticle sizes [63]. Thus, it was expected that both FWHM and the intensity of the resonance peaks were affected by increasing the Au-G hybrid nanoparticle diameters from 40 to 60 nm as confirmed in Fig. 6a,b.

As can be seen from Fig. 6b, the extinction intensity was recorded as 70 and 55 % in the hybrid nanostructures with a diameter of 60 nm and graphene thicknesses of 5 and 7 nm, respectively. As it is evident from Fig. 6a, it is clear that the resonance mode at maximum extinction intensity offers narrower width in the hybrid nanostructure with larger diameter. The FWHM of the hybrid nanostructure with hybrid nanoparticle size of 40 nm and graphene thickness of 3 nm was calculated as large as 8.5 nm, while the FWHM of the hybrid nanostructure with nanoparticle size of 60 nm and graphene thicknesses of 5 and 7 nm was calculated as 2.9 and 2.5 nm, respectively.

It can be concluded that the optimum Au-G hybrid nanoparticle diameter and graphene shell thickness which offer narrower resonance bandwidth in a hybrid nanostructure sensor are 60 and 7 nm, respectively, at 300 nm structural periodicity which could result in larger FOM of the designed sensor.

Measurement Sensitivity as a Liquid Sensor

Periodic Au-G hybrid nanostructure arrays with optimum structural parameters (i.e., nanoparticle size (D) of 60 nm, graphene thickness of 7 nm as encapsulating layer, and structural period of 300 nm) were employed as refractive index sensor. Water with refractive index of 1.333 was chosen as

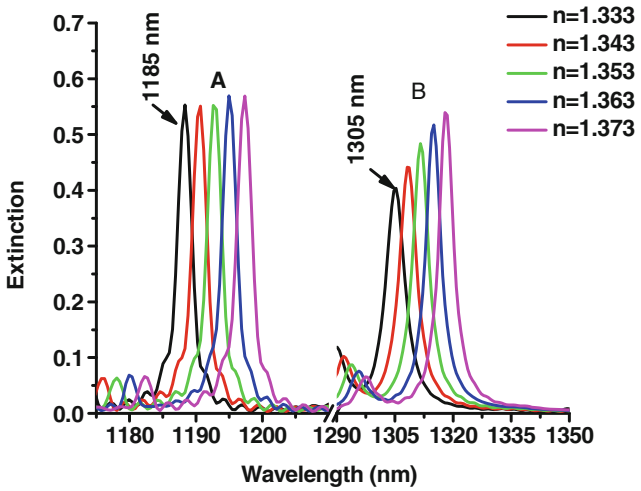

Fig. 7 The recorded extinction spectra of the Au-G hybrid nanostructure of 60-nm nanoparticle diameter, 7 nm thick graphene shell, and 300 nm structural periodicity. The incident electric field amplitude was fixed at 1 V/m

reference liquid, and target liquid refractive indices were varied in the range of 1.333 to 1.373.

The sensing performance of the proposed periodic nanostructure was investigated by using water as reference liquid and two different properties of resonance peaks: resonance wavelength shift ($\Delta\lambda$) and resonance intensity shift (ΔI) at different refractive indices of the target liquids.

Figure 7 shows the recorded extinction spectra of the hybrid nanostructure with the optimum structural parameters at different refractive indices in the range of 1.333 to 1.373. As can be seen from this figure, there are two major resonance wavelengths which are labeled as A (λ = 1188 nm) and B (λ = 1305 nm). These two resonance modes were used for wavelength sensitivity (S_λ) and intensity sensitivity (S_I) measurements.

The wavelength sensitivity, S_λ, is calculated by dividing the resonance wavelength shift ($\Delta\lambda = \lambda_{res} - \lambda_{ref}$) by the refractive index change ($\Delta n = n_t - n_{ref}$), while the intensity sensitivity [50] was calculated by dividing the resonance intensity shift ($\Delta I = I_{res} - I_{ref}$) by the refractive index change ($\Delta n = n_t - n_{ref}$).

From Fig. 8a, it is clear that by increasing the hybrid nanostructure diameter, the sensitivity of the designed structure was decreased over the refractive index change from 1.333 to 1.373. Furthermore, it was found that larger graphene thickness resulted in larger sensitivity at a fixed hybrid nanoparticle diameter of 60 nm as shown in Fig. 8b. From Fig. 8c, it is also evident that by increasing the refractive index of the target liquid from 1.333 to 1.373, the resonance wavelength was red shifted from 1188 to 1197 nm and from 1305 to 1318 nm, respectively, for both resonance modes of A and B.

Both the calculated wavelength sensitivity and intensity sensitivity and FOM of the Au-G hybrid nanostructure are

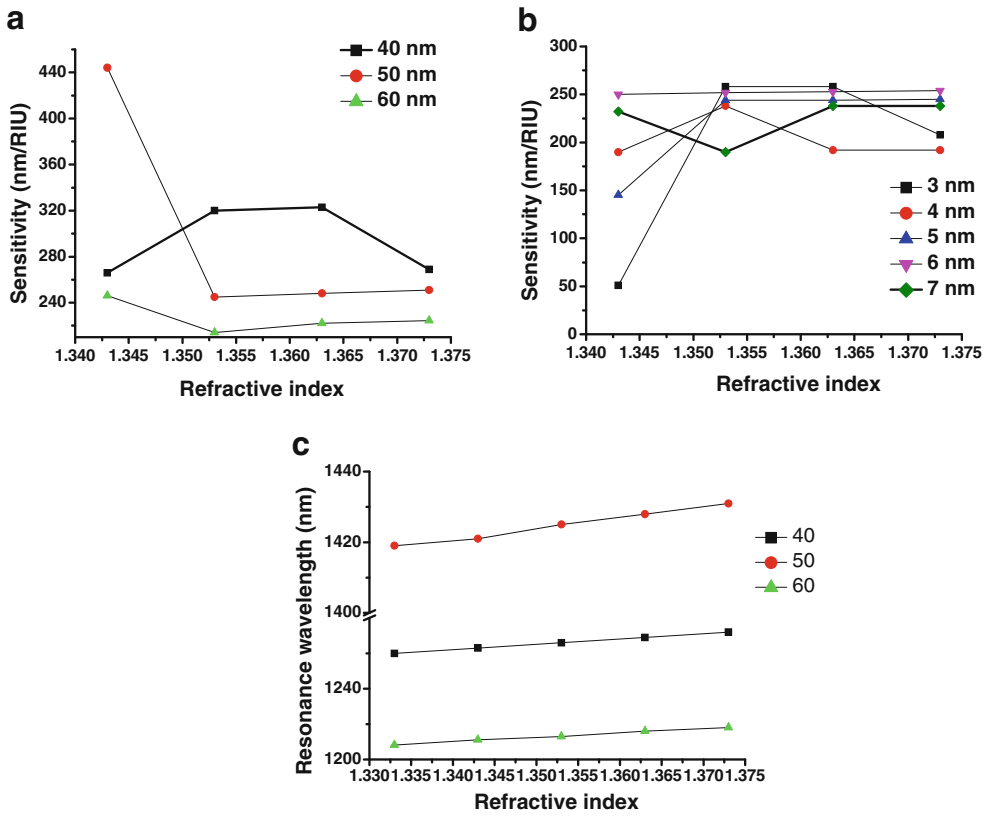

Fig. 8 **a** Sensitivity of the Au-G hybrid nanostructure at different sizes over refractive index change. **b** Sensitivity of the Au-G hybrid nanostructure with size of 60 nm at different graphene shell thicknesses. **c** Resonance wavelength (bonding mode) shift as refractive index change from 1.333 to 1.373 for the Au-G hybrid nanostructure at different sizes at fixed shell thickness of 7 nm

Table 2 Resonance wavelength, bulk resonance, intensity sensitivity, FWHM, and FOM of resonance modes in an Au-G hybrid nanostructure with an Au diameter of 60 nm, graphene thickness of 7 nm, and structural periodicity of 300 nm. The incident electric field amplitude was fixed at 1 V/m

Resonance peak	$\lambda_{res.}$ (nm)	S_λ (nm/RIU)	S_I (RIU^{-1})	FWHM (nm)	FOM$_\lambda$	FOM$_I$
A	1190	200	0.3	2.64	75.75	0.11
	1193	250	0.2	2.69	92.94	0.07
	1195	233	1.7	2.27	102.64	0.75
	1197	225	–	2.69	83.64	–
B	1308	300	3.9	5.20	57.69	0.75
	1312	350	4.2	4.80	72.91	0.47
	1315	333	3.3	4.61	72.23	0.72
	1318	325	2.2	4.55	71.43	0.48

summarized in Table 2. As detailed in this table, the calculated FOM from the S_λ was increased in the range of 57.69 to 102.64 on increasing the refractive index of the target liquid from 1.333 to 1.373 which shows a big improvement in the sensor performance compared to the previously reported one based on the LSPR sensors [6, 32], nanohole arrays [54], and metal-insulator-metal nanobelt structures [37, 52, 54].

On the other hand, the FOM obtained from S_I sensitivity was increased from 0.07 to 0.75 by increasing the refractive index of the target liquid which increases the capability of the designed sensor to measure two different properties instead of one and hence improves the quality and reliability of the fabricated device based on the proposed technology.

Conclusion

The effect of periodicity, metallic nanoparticle size, and graphene shell thickness of the Au-graphene hybrid nanostructure on the optical properties, sensitivity, and FOM of an Au-graphene hybrid nanosensor were studied numerically. Encapsulating the Au nanoparticles with a multilayer layer of graphene enhanced the extinction intensity (absorption) at the NIR region followed by a narrow resonance mode with FWHM as low as 2 nm that increased the FOM of the proposed sensor as high as 103 which shows a significant improvement in the Au nanoparticle-based sensors by incorporating a thin layer of graphene.

The results shown here confirm that resonance properties strongly depend on the hybrid nanostructure size and graphene shell thickness. The resonance wavelength was reduced toward smaller wavelengths by increasing the graphene shell thickness. It was also shown that the proposed sensor is capable of measuring two different types of sensitivities based on the resonance wavelength shift and resonance intensity shift which give this sensor a unique applicability for a variety of applications.

Acknowledgments RA acknowledges Taibah University, Saudi Arabia, for the financial support. RA, MI, and MY would like to acknowledge the National Science and Engineering Research Council of Canada (NSERC) for the financial support.

References

1. Brolo AG (2012) Plasmonics for future biosensors. Nat Photonics 6(11):709–713
2. Homola J (2008) Surface plasmon resonance sensors for detection of chemical and biological species. Chem Rev 108:462–493
3. Toma M, Cho K, Wood JB, Corn RM (2013) Gold nanoring arrays for near infrared plasmonic biosensing. Plasmonics 9(4):765–772
4. Liang Y, Lu M, Chu S, Li L, Peng W (2015) Tunable plasmonic resonances in the hexagonal nanoarrays of annular aperture for biosensing. Plasmonics 11(1):205–212
5. Sherry LJ, Chang SH, Schatz GC, Duyne RPV (2005) Localized surface plasmon resonance spectroscopy of single silver nanocubes. Nano Lett 5:2034–2038
6. Mayer KM, Hafner JH (2011) Localized surface plasmon resonance sensors. Chem Rev 111(6):3828–3857
7. Anker JN, Hall WP, Lyandres O, Shah NC, Zhao J, Duyne RPV (2008) Biosensing with plasmonic nanosensors. Nat Mater 7
8. Bukasov R, Shumaker-Parry JS (2007) Highly tunable infrared extinction properties of gold nanocrescents. Nano Lett 7(4)
9. Wang H, Brandl DW, Le F, Nordlander P, Halas NJ (2006) Nanorice: a hybrid plasmonic nanostructure. Nano Lett 6:827–832
10. Svedendahl M, Chen S, Dmitriev A, Ka M (2009) Refractometric sensing using propagating versus localized surface plasmons: a direct comparison. Nano Lett 9(12):4428–4433
11. Shen Y, Zhou J, Liu T, Tao Y, Jiang R, Liu M, Xiao G, Zhu J, Zhou ZK, Wang X, Jin C, Wang J (2013) Plasmonic gold mushroom arrays with refractive index sensing figures of merit approaching the theoretical limit. Nat Commun 4:2381
12. Y.A.K. Imogen M. Pryce, Koray Aydin, and Harry A. Atwater, Compliant metamaterials for resonantly enhanced infrared absorption spectroscopy and refractive index sensing. ACS Nano, 2011. 5(10): 8167–8174.
13. Verellen N, Van Dorpe P, Huang C, Lodewijks K, Vandenbosch GA, Lagae L, Moshchalkov VV (2011) Plasmon line shaping using nanocrosses for high sensitivity localized surface plasmon resonance sensing. Nano Lett 11(2):391–397
14. Lassiter JB, Sobhani H, Fan JA, Kundu J, Capasso F, Nordlander P, Halas NJ (2010) Fano resonances in plasmonic nanoclusters: geometrical and chemical tunability. Nano Lett 10(8):3184–3189
15. Auguie B, Barnes WL (2008) Collective resonances in gold nanoparticle arrays. Phys Rev Lett 101(14):143902

16. Kravets VG, Schedin F, Grigorenko AN (2008) Extremely narrow plasmon resonances based on diffraction coupling of localized plasmons in arrays of metallic nanoparticles. Phys Rev Lett 101(8): 087403
17. Vecchi G, Giannini V, Gómez Rivas J (2009) Surface modes in plasmonic crystals induced by diffractive coupling of nanoantennas. Phys Rev B 80(20):201401
18. Zhou W, Odom TW (2011) Tunable subradiant lattice plasmons by out-of-plane dipolar interactions. Nat Nanotechnol 6(7):423–427
19. Hicks EM, Zou S, Schatz GC, Spears KG, Duyne RPV (2005) Controlling plasmon line shapes through diffractive coupling in linear arrays of cylindrical nanoparticles fabricated by electron beam lithography. Nano Lett 5(6):1065–1070
20. Wang D, Yang A, Hryn AJ, Schatz GC, Odom TW (2015) Superlattice plasmons in hierarchical Au nanoparticle arrays. ACS Photonics 2(12):1789–1794
21. Kreibig U, Vollmer M (1995) Optical properties of metal clusters, vol 25. Springer, New York
22. Link S, El-Sayed MA (2000) Shape and size dependence of radiative, non-radiative and photothermal properties of gold nanocrystals. Int Rev Phys Chem 19(3):409–453
23. Yan F, Xia H, Avouris P (2013) The interaction of light and graphene: basics, devices, and applications. Proc IEEE 101:1717–1731
24. Navas MP, Soni RK (2015) Laser-generated bimetallic Ag-Au and Ag-Cu core-shell nanoparticles for refractive index sensing. Plasmonics 10(3):681–690
25. Gan X, Mak KF, Gao Y, You Y, Hatami F, Hone J, Heinz TF, Englund D (2012) Strong enhancement of light–matter interaction in graphene coupled to a photonic crystal nanocavity. Nano Lett 12(11):5626–5631
26. Ju L, Geng B, Horng J, Girit C, Martin M, Hao Z, Bechtel HA, Liang X, Zettl A, Shen YR (2011) Graphene plasmonics for tunable terahertz metamaterials. Nat Nanotechnol 6(10):630–634
27. Alaee R, Farhat M, Rockstuhl C, Lederer F (2012) A perfect absorber made of a graphene micro-ribbon metamaterial. Opt Express 20(27):28017–28024
28. Nikitin AY, Guinea F, Garcia-Vidal FJ, Martin-Moreno L (2012) Surface plasmon enhanced absorption and suppressed transmission in periodic arrays of graphene ribbons. Phys Rev B 85(8):081405
29. Thongrattanasiri S, Koppens FH, Garcia de Abajo FJ (2012) Complete optical absorption in periodically patterned graphene. Phys Rev Lett 108(4):047401
30. Zhao B, Zhao JM, Zhang ZM (2014) Enhancement of near-infrared absorption in graphene with metal gratings. Appl Phys Lett 105(3): 031905
31. Liu Y, Chadha A, Zhao D, Piper JR, Jia Y, Shuai Y, Menon L, Yang H, Ma Z, Fan S, Xia F, Zhou W (2014) Approaching total absorption at near infrared in a large area monolayer graphene by critical coupling. Appl Phys Lett 105(18):181105
32. Maurer T, Nicolas R, Lévêque G, Subramanian P, Proust J, Béal J, Schuermans S, Vilcot JP, Herro Z, Kazan M, Plain J, Boukherroub R, Akjouj A, Djafari-Rouhani B, Adam PM, Szunerits S (2013) Enhancing LSPR sensitivity of Au gratings through graphene coupling to Au film. Plasmonics 9(3):507–512
33. Martinsson E, Sepulveda B, Chen P, Elfwing A, Liedberg B, Aili D (2013) Optimizing the refractive index sensitivity of plasmonically coupled gold nanoparticles. Plasmonics 9(4):773–780
34. Martinsson E, Shahjamali MM, Enander K, Boey F, Xue C, Aili D, Liedberg B (2013) Local refractive index sensing based on edge gold-coated silver nanoprisms. J Phys Chem C 117(44):23148–23154
35. Mayer KM, Hao F, Lee S, Nordlander P, Hafner JH (2010) A single molecule immunoassay by localized surface plasmon resonance. Nanotechnology 21(25):255503
36. Larsson EM, Alegret J, Käll M, Sutherland DS (2007) Sensing characteristics of NIR localized surface plasmon resonances in gold nanorings for application as ultrasensitive biosensors. Nano Lett 7(5):1256–1263
37. Irannejad M, Cui B, Yavuz M (2015) Optical properties and liquid sensitivity of Au-SiO2-Au nanobelt structure. Plasmonics 11(1):1–9
38. Yang B, Wu T, Yang Y, Zhang X (2015) Tunable subwavelength strong absorption by graphene wrapped dielectric particles. J Opt 17(3):035002
39. Christensen T, Jauho A-P, Wubs M, Mortensen NA (2015) Localized plasmons in graphene-coated nanospheres. Phys Rev B 91(12):125414
40. Li Q, Zhang Z (2016) Bonding and anti-bonding modes of plasmon coupling effects in TiO2-Ag core-shell dimers. Sci Rep 6:19433
41. Sreejith S, Joseph J, Nguyen KT, Murukeshan VM, Lye SW, Zhao Y (2015) Graphene oxide wrapping of gold–silica core–shell nanohybrids for photoacoustic signal generation and bimodal imaging. ChemNanoMat 1(1):39–45
42. Han TH, Lee WJ, Lee DH, Kim JE, Choi EY, Kim SO (2010) Peptide/graphene hybrid assembly into core/shell nanowires. Adv Mater 22(18):2060–2064
43. Staudinger C, Borisov SM (2015) Long-wavelength analyte-sensitive luminescent probes and optical (bio) sensors. Methods Appl Fluoresc 3(4):042005
44. Li J, Chen K, Liu H, Cheng K, Yang M, Zhang J, Cheng JD, Zhang Y, Cheng Z (2012) Activatable near-infrared fluorescent probe for in vivo imaging of fibroblast activation protein-alpha. Bioconjug Chem 23(8):1704–1711
45. Blake P, Ahn W, Roper DK (2010) Enhanced uniformity in arrays of electroless plated spherical gold nanoparticles using tin presensitization. Langmuir 26(3):1533–1538
46. Shim J, Yun JM, Yun T, Kim P, Lee KE, Lee WJ, Ryoo R, Pine DJ, Yi G-R, Kim SO (2014) Two-minute assembly of pristine large-area graphene based films. Nano Lett 14(3):1388–1393
47. Irannejad M, Alyalak W, Burzhuev S, Brzezinski A, Bo MCY (2015) Engineering of Bi−/mono-layer graphene film using reactive ion etching. Trans Electr Electron Mater 16(4):169–172
48. Campos LC, Manfrinato VR, Sanchez-Yamagishi JD, Kong J, Jarillo-Herrero P (2009) Anisotropic etching and nanoribbon formation in single-layer graphene. Nano Lett 9(7):2600–2604
49. Wannemacher R (2001) Plasmon supported-transmission of light through nanometric holes in metallic thin films. Opt Commun 195:107–118
50. Cattoni A, Ghenuche P, Haghiri-Gosnet AM, Decanini D, Chen J, Pelouard JL, Collin S (2011) Lambda(3)/1000 plasmonic nanocavities for biosensing fabricated by soft UV nanoimprint lithography. Nano Lett 11(9):3557–3563
51. Francs GC d, Molenda D, Fischer UC, Naber A (2005) Enhanced light confinement in a triangular aperture: experimental evidence and numerical calculations. Phys Rev B 72(16)
52. Irannejad M, Cui B (2013) Effects of refractive index variations on the optical transmittance spectral properties of the nano-hole arrays. Plasmonics 8(2):1245–1251
53. Irannejad M, Yavuz M, Cui B (2013) Finite difference time domain study of light transmission through multihole nanostructures in metallic film. Photonics Res 1(4):154
54. Irannejad M, Zhang J, Yavuz M, Cui B (2013) Numerical study of optical behavior of nano-hole array with non-vertical sidewall profile. Plasmonics 9(3):537–544
55. Haynes WM (2014) CRC handbook of chemistry and physics. CRC Press, Boca Raton, Fl
56. Falkovsky LA (2008) Optical properties of graphene and IV–VI semiconductors. Physics-Uspekhi 9(51):887–898
57. Mesh refinement options 2015 Available from: https://kb.lumerical.com/en/index.html?ref_sim_obj_mesh_refinement_options.html.

58. Chen Y, Wu H, Li Z, Wang P, Yang L, Fang Y (2012) The study of surface plasmon in Au/Ag core/shell compound nanoparticles. Plasmonics 7(3):509–513
59. E. Prodan, C. Radloff, N.J. Halas, P. Nordlander, *A hybridization model for the plasmon response of complex nanostructures.* Science 302
60. Radloff C, Halas NJ (2004) Plasmonic properties of concentric nanoshells. Nano Lett 4(7):1323–1327
61. Lal S, Link S, Halas NJ (2007) Nano-optics from sensing to waveguiding. Nat Photonics 1:641–648
62. S.A. Maier, *Plasmonics: fundamentals and applications*. 2007: Springer Science & Business Media.
63. Kofke MJ, Waldeck DH, Walker GC (2010) Composite nanoparticle nanoslit arrays: a novel platform for LSPR mediated subwavelength optical transmission. Opt Express 18(8):7705–7713